Application of Image Processing for Simulation of Mechanical Response of Multi–Length Scale Microstructures of Engineering Alloys

ARUN M. GOKHALE and SHICHEN YANG

Microstructures of engineering alloys often contain features at widely different length scales. In this contribution, a digital image processing technique is presented to incorporate the effect of features at higher length scales on the damage evolution and local fracture processes occurring at lower length scales. The method is called M-SLIP: Microstructural Scale Linking by Image Processing. The technique also enables incorporation of the real microstructure at different length scales in the finite element (FE)-based simulations. The practical application of the method is demonstrated *via* FE analysis on the microstructure of an aluminum cast alloy (A356), where the length scales of micropores and silicon particles differ by two orders of magnitude. The simulation captures the effect of nonuniformly distributed micropores at length scales of 200 to 500 μm on the local stresses and strains around silicon particles that are at the length scales of 3 to 5 μm. The procedure does not involve any simplifying assumptions regarding the microstructural geometry, and therefore, it is useful to model the mechanical response of the *real* multi–length scale microstructures of metals and alloys.

I. INTRODUCTION

MICROSTRUCTURES often contain features at length scales ranging from nanometers to millimeters. These features have complex geometry, their locations and orientations are usually nonuniform, and strong spatial correlation often exists among different types of features. In such complex microstructures, deformation and fracture processes are usually governed by several types of microstructural features that may be present at widely different length scales. Further, damage evolution and local fracture processes at lower length scales are affected by the amount, size distribution, and spatial arrangement of features at higher length scales, and vice versa. The "coupling effect" of the microstructural features at widely different length scales, and their complex geometry, creates serious difficulties in modeling the mechanical response of *real* multi–length scale microstructures. For example, consider a typical microstructure of A356 cast alloy (an Al-Si-Mg base alloy containing 7 wt pct Si and 0.3 wt pct Mg) shown at different magnifications in Figure 1 to illustrate the presence of microstructural features at widely different length scales. Figure 1(a) shows a very low magnification macrograph that depicts nonuniformly distributed micropores, which is typical in cast microstructure. Figure 1(b) shows the microstructure at somewhat higher magnification, illustrating that the micropore sizes are on the order of 50 to 300 μm and interpore distances are on the order of 300 to 500 μm ($\sim$half a millimeter). The microstructural space between micropores contains features at lower length scales. Figure 1(c) is a higher magnification micrograph depicting the presence of aluminum-rich dendrite cells whose sizes are on the order of 20 to 70 μm and silicon-rich interdendrite regions. Figure 1(d) is a high magnification micrograph (500X) which shows the silicon particles in the interdendritic regions. The Si particles have sizes on the order of 1 to 4 μm, and the interparticle distances between the Si particles are on the order of 3 to 5 μm. Therefore, the length scales of the micropores and Si particles differ by about two orders of magnitudes. In this alloy, microstructural features such as Mg_2Si precipitates are present at the submicron and lower length scale regimes.

An important damage mechanism in A356 cast alloy is gradual fracture and debonding of silicon particles.[1–4] Such damage evolution is typical of many alloys containing particulate phases. Fracture and debonding of Si particles (Figure 2(a)) initiates at stresses slightly above the yield stress.[1] The extent of this damage increases with the applied stress.[1–4] At sufficiently high stresses, microcracks link the fractured/debonded Si particles in the interdendritic regions, and ultimately linkage of such microcracks between neighboring micropores leads to fracture (see Figure 2(b)). The presence of micropores obviously alters the local stress distribution around the Si particles, and affects their damage evolution; and therefore, it should be accounted for in modeling damage and fracture of Si particles. The effect of micropores on the damage evolution of Si particles depends on the volume fraction of micropores, their size distribution, *and* their *spatial arrangement*. Therefore, to model the fracture and debonding of Si particles (*i.e.*, damage evolution) and local fracture processes in the interdendritic regions which are at the length scales of 3 to 6 μm, one must account for the effect of micropores that are present at the length scales of 300 to 500 μm. The spatial arrangement of micropores is usually nonuniform (Figures 1(a) and (b)), and depending on the casting process, they exhibit a wide range of shapes and sizes.[2] The silicon particles are also nonuniformly distributed (they are present only in the interdendritic regions), and they exhibit a wide range of sizes and shapes as well. Further, larger and elongated Si particles are expected to fracture and debond preferentially.[1,4,5] Such complexities are encountered in microstructures of almost all alloys of

ARUN M. GOKHALE, Professor, and SHICHEN YANG, Graduate Student, are with the Department of Materials Science and Engineering, Georgia Institute of Technology, Atlanta, GA 30332-0245.
Manuscript submitted November 3, 1998.

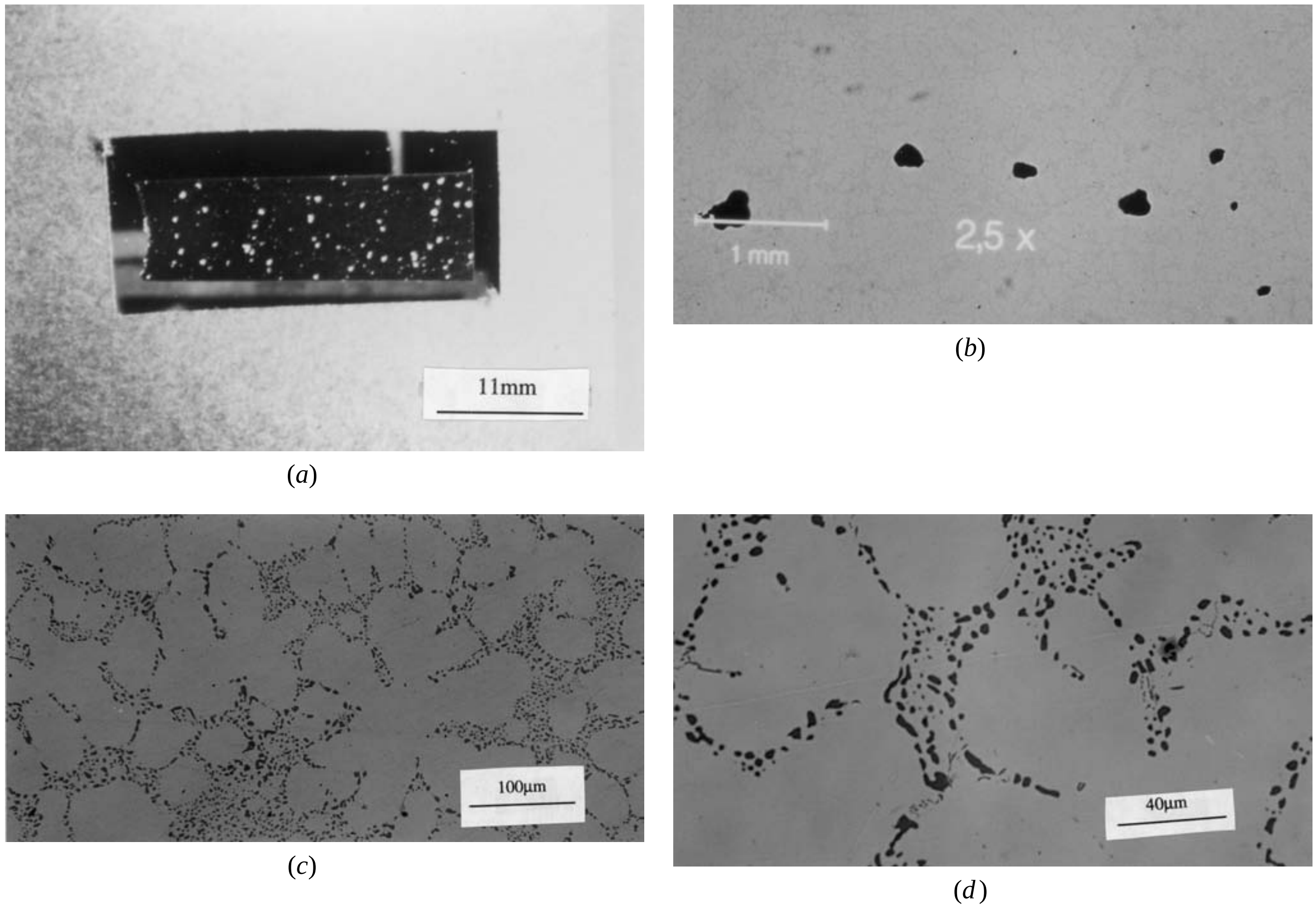

Fig. 1—(*a*) Micrograph depicting the nonuniform distribution of micropores in the Al-Si-Mg cast alloy (A356). (*b*) Micrograph showing the sparsely distributed micropores with size on the order of 50 to 300 μm and interpore distance on the order of 300 to 500 μm. (*c*) Micrograph depicting the aluminum-rich dendrite cells and the silicon-rich interdendritic regions in the Al-Si-Mg cast alloy (A356). (*d*) High magnification micrograph illustrating the clustering of silicon particles with size on the order of 1 to 4 μm in the interdendritic region.

practical importance, and they should be accounted for in finite element (FE)-based modeling of fracture and damage in such microstructures.

Computational mechanics based modeling and simulations of damage evolution and fracture processes present unique means for analyzing fracture at micro- and mesoscales. There have been significant developments in the computational micromechanics and damage mechanics techniques for FE-based simulation of fracture processes.[6–10] However, micromechanics and damage mechanics based numerical modeling studies reported in the literature often *ignore* the complex details of the geometry of *real* material microstructures; with few notable exceptions, most of the simulations are performed on the idealized microstructures having uniformly distributed monosized microstructural features of simple shapes (for example, aligned cylinders or spheres). In such simulations, effect of microstructural features at *lower* length scales on the deformation and fracture processes at higher length scales is incorporated *via* well-known "homogenization" techniques.[11,12,13] However, homogenization procedures are not useful to model the effect of microstructural features at higher length scales on the damage and fracture processes at lower length scales. Further, homogenization techniques ignore nonuniform, nonrandom spatial arrangements of microstructural features and spatial correlation among the microstructural features at different length scales. The effects of microstructural extrema on the mechanical response[14] are not captured in the numerical simulations. Therefore, such FE-based simulations may be useful for the parametric studies, but they cannot accurately simulate the mechanical response of *real* multi–length scale microstructures in which the microstructural features have complex geometry.

Development of practical FE-based methodology to model deformation and fracture of multi–length scale microstructures of engineering alloys is an unsolved complex problem, whose solution will require contributions of scientists from many different disciplines. In the present work, we focus on two important issues related to this complex problem, namely, (1) how to incorporate the true size, shape, and orientation distribution, *and* **spatial arrangements** of the microstructural features at different length scales in the FE-based simulations; and (2) how to incorporate the effect of microstructural features at higher length scales on local stresses and strains distributions, and fracture processes at lower length scale in FE-based simulations on multi–length scale microstructure. These questions are addressed *via* a novel digital image analysis-based approach. The methodology involves combination digital image processing techniques such as "montage" creation,[15,16] compression of

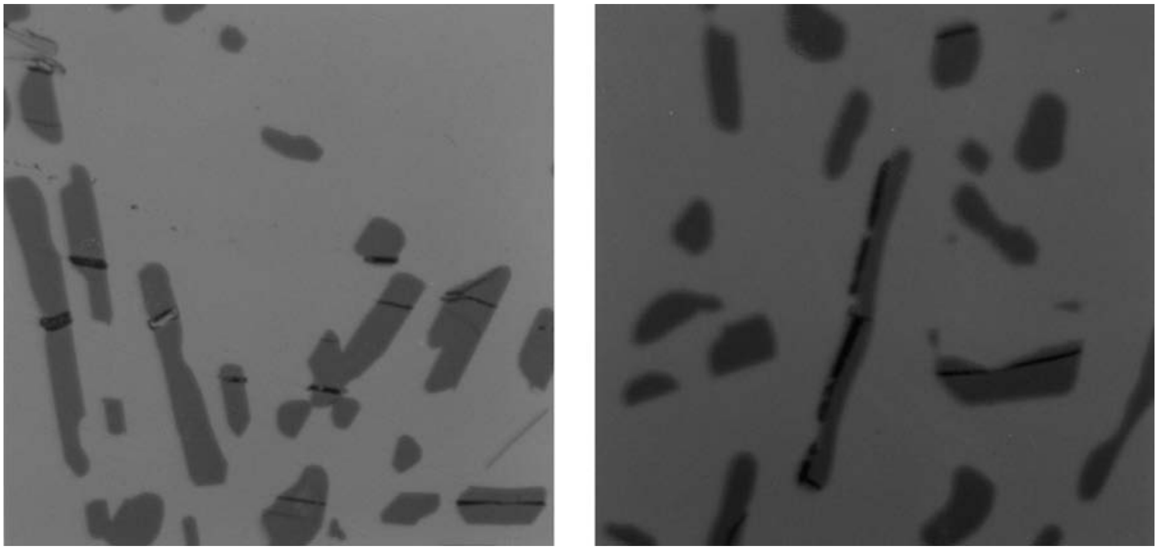

Fractured particles Debonded particles

(*a*)

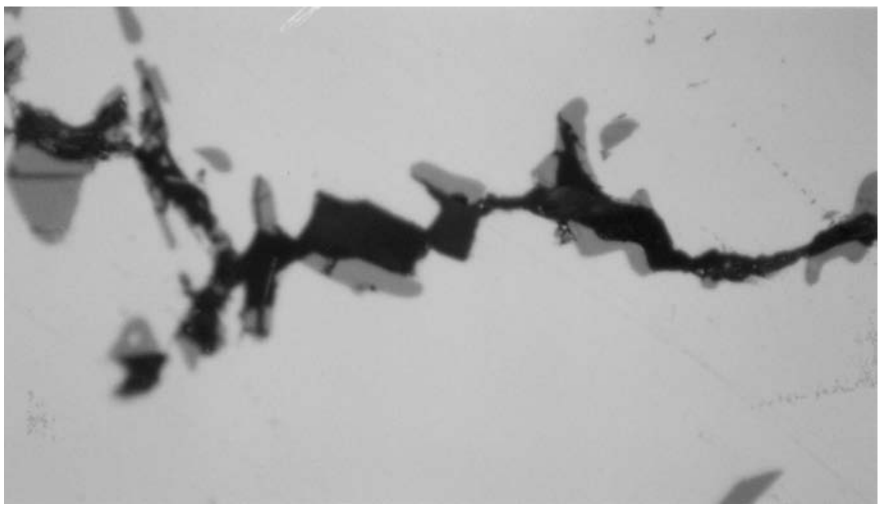

(*b*)

Fig. 2—(*a*) Micrographs showing the fractured and debonded silicon particles in the Al-Si-Mg cast alloy (A356). (*b*) Micrograph depicting the linkage of the fractured/debonded silicon particles to form microcracks in the Al-Si-Mg cast alloy (A356).

digital microstructural images, and use of the digital image montages for the FE-based simulations of mechanical response. The methodology is illustrated *via* its application to the FE-based analysis on complex microstructure of a cast A356 Al-alloy. However, the basic technique is completely general, and it is applicable to any microstructure. In this article, the emphasis is on the development of the image processing technique and demonstration of its utility for FE analysis, rather than on detailed damage mechanics/micromechanics based computations from the FE-based simulations of stress and strain distributions. These aspects will be presented in another contribution. The next section of the article gives background on earlier work in this area. The subsequent section describes the digital image analysis procedures for creation of high-resolution large-area "microstructural" montage and image compression to link the length scales. This technique is then applied to the complex microstructure of an A356 alloy to link the microstructural length scales that differ by two orders of magnitude in FE-based simulations.

II. BACKGROUND

In few pervious studies, attempts have been made to perform the FE-based simulations directly on the digital microstructural images. To incorporate the complexities of the spatial arrangement of features in real microstructure, Brokenbrough and Hunt[17] captured the digital image of one microstructural field of an Al-Si alloy and performed the FE analysis to compute the strain and stress distributions around silicon particles at different locations in the microstructural field examined. The shape of each silicon particle in the microstructural field was approximated by equivalent circle in the geometric model of the FE analysis. These authors concluded that the nonuniform spatial arrangement of silicon particles affects the local stress and strain distributions around silicon particles. However, Brokenbrough and Hunt did not incorporate the effect of the features such as micropores, that may be present at much higher length scales, on the local stress and strain distributions around the silicon particles, and therefore, their analysis did not involve linking of microstructural length scales. Wulf *et al.*[18] simulated crack path in a composite consisting of SiC particles in an aluminum alloy matrix. In their simulations, one microstructural field containing ten SiC particles was considered as representative of the microstructure. The digital image of this microstructural field was embedded in an effective homogenous medium, and Rice and Tracy damage parameter[19] was utilized for local failure criterion to simulate the crack path. Wulf *et al.* concluded that the simulated crack path was in good agreement with the actual experimental crack path through the specimen. Recently, Al-Ostazz and Jasiuk[20] performed experimental and simulation studies on crack path through transversely loaded aluminum plates containing macroscopic holes. Their experiments showed that the different plates having same nominal sizes and spatial arrangement of holes did not exhibit the same fracture path, although FE-based simulation on the same "macrostructure" predicted a unique fracture path. Al-Ostaz and Jasiuk did not incorporate the underlying microstructure of the aluminum alloy plate in their FE simulations. It is likely that the differences in the experimental crack paths in different plates may have been due to the local variations in the microstructure from one plate to another. The actual spatial arrangement of macroscopic holes in the aluminum plates was captured in the finite element analysis of Al-Ostaz and Jasiuk, but the effect of underlying microstructure which may contain widely different length scale features was not considered. These difficulties can be resolved by using the image processing technique presented in the next section.

III. MICROSTRUCTURAL SCALE LINKING BY IMAGE PROCESSING

The geometric complexities of the real material microstructures can be incorporated in the FE studies of the mechanical response of the microstructure, simply by "embedding" microstructural images in the FE analysis model. However, it is not sufficient to perform the FE analysis on only one microstructural field, as it has been done in the earlier studies, because there are statistical variations in the microstructure from one field to another, and a single randomly selected field cannot be regarded as representative of the whole microstructure. It is necessary to repeat the FE analysis on a sufficiently large number of microstructural fields to arrive at the distribution of mechanical responses that include both the average and the extreme behavior of the system.

To incorporate the effect of spatial arrangement of microstructural features at different length scales in the FE-based simulations, a sufficiently large region of microstructure must be observed. In the A356 alloy, to observe the spatial pattern of the micropores, it would be necessary to observe the microstructure at the magnification of about 25X. However, at this magnification, the silicon particles are not resolved as their sizes are much finer, and therefore, these fine features cannot be included the FE analysis, if low magnification digital images are used. On the other hand, if the microstructure is observed at sufficiently high magnification (say, 500X) where the silicon particles are clearly resolved, the field of view may contain just one or two micropores, and some microstructural fields may not contain any micropores at all. This is because the area of one microstructural frame observed at 500X is 400 times smaller than a frame observed at 25X (the area of the microstructural frame observed is inversely proportional to the square of the magnification). As the high magnification view depicts very small region of microstructure, the spatial arrangement of coarse features such as micropores cannot be captured, and consequently, the FE analysis on high magnification microstructural fields does not appropriately account for the effects of the coarse features such as micropores. Therefore, at any one fixed magnification level, both the coarse and the fine microstructural features cannot be studied and their interactions cannot be included in the FE analysis, by using the conventional microscopy and image analysis. We propose to resolve this difficulty by using the image processing techniques to create large-area high-magnification microstructural montage. The procedure involves the following steps: (1) grabbing of very large number (say 400 to 600) of overlapping contiguous microstructural fields at a high magnification (say, 500X), and creation of a "seamless" montage of these contiguous fields by "pixel by pixel matching" at the overlapping borders; (2) digital compression of the microstructural montage; and (3) incorporation of digital image montage and their compressions to generate cascade of FE schemes at different length scales. These steps are described in the following subsections.

A. *Creation of Microstructural Montage*

Louis and Gokhale[15,16] have developed an image analysis procedure for creating seamless microstructural montage of a large number of contiguous microstructural fields for quantitative characterization of spatial arrangement of microstructural features, which is briefly described here, as it relates to the present work. First, a suitable magnification is selected, where the microstructural features of the finest length scale of interest are clearly resolved. At this magnification level, the first image frame (field of view) is selected arbitrarily and stored in the memory of the image analyzing computer. The right border (having about 50 pixel width) of this image is pasted on the left edge of the next approximately contiguous live image frame (field of view), the microscope stage is moved and adjusted so as to fit the right border of the previous frame to the left edge of the live image within about 10 to 20 pixels; this rough matching is done manually by the operator. At this point, the image of the live frame is grabbed, and translated pixel by pixel until it perfectly matches with the left border of the previous field displayed on the screen* (Figure 3(a)). Once the satisfactory match (within one pixel) is achieved, the second image frame is stored. The same procedure is continued with the successive image frames. In this manner, a seamless montage of any number of precisely contiguous image fields can be created and stored in the computer; the upper limit on the number of image fields is set only by the hard disk memory, and not by the image analysis procedure. Figure 3(b) shows a

*Note that the commands for image translation by fixed number of pixels are available on a majority of image analyzers.

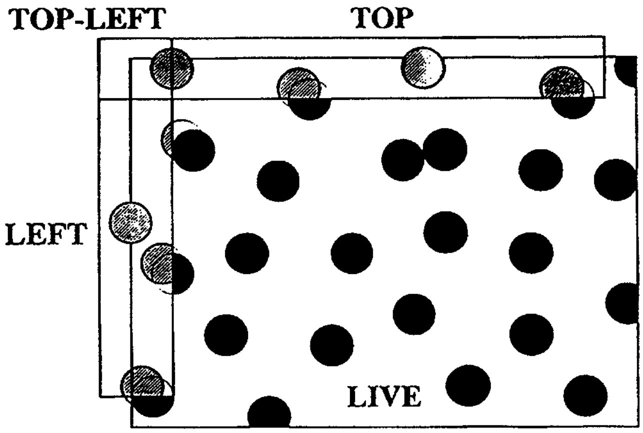

(*a*)

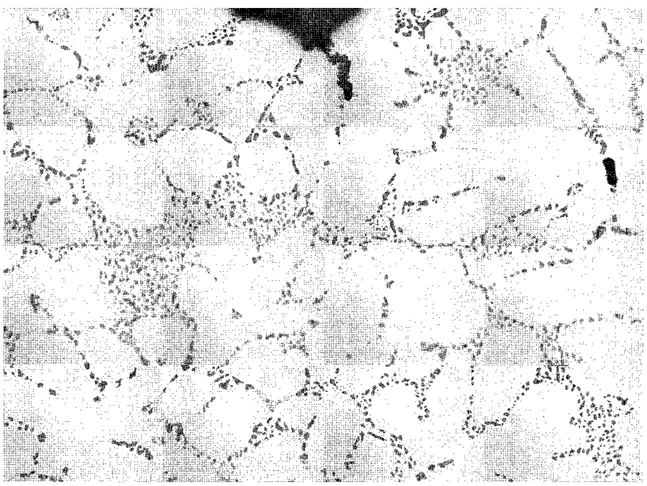

(*b*)

Fig. 3—(*a*) Schematic drawing showing the matching of two contiguous microstructural fields. (*b*) Montage of 16 contiguous microstructural fields grabbed at 500X (compressed for demonstration).

microstructural montage of 16 microstructural fields of cast A356 alloy grabbed at 500X created in this manner (the montage is compressed for display). In this montage, the adjoining microstructural fields can be distinguished due to slight differences in the gray levels from one field to another; however, the microstructural features at the borders of the adjoining fields are perfectly matched (within one pixel), and therefore the montage is "seamless." The pixel by pixel matching and the resulting "seamless" character of the montage are absolutely essential for the FE analysis; otherwise, unmatched microstructural features at the borders of the microstructural fields can result in artificial discontinuities in the microstructure, that can change the simulated local strain and stress distributions. The effort involved in the creation of microstructural montage can be significantly reduced by using automatic programmable specimen stage and auto-focus attachments for microscope. In such a case, the overlapping fields can be automatically grabbed, and the operator interaction is needed only for the "pixel by pixel" matching at the microstructural frame borders. The montage can be as large as desired: the microstructural fields in the montage may cover the whole specimen. Therefore, the montage contains all the microstructural information (small range, intermediate range, long range, and extrema) at high resolution.

In principle, one can overlay a very fine FE mesh (the mesh size has to be much smaller than the microstructural features of finest length scale) on the whole microstructural montage and perform the FE analysis, but such fine meshing over large area of the montage will require enormous time and effort, particularly, if the meshing is to be done manually. Further, such a FE scheme would be computationally very inefficient, and in some cases, it may not be practically feasible. To resolve these difficulties, we propose digital image compression, and sequential cascading to facilitate the generation of a "cascade" of FE schemes at different resolution levels.

B. *Digital Image Compression*

Note that each microstructural field of the montage is at a sufficiently high magnification where the microstructural features of finest length scale of interest are clearly resolved. For the present A356 alloy microstructure, the finest features of interest are the silicon particles and they are clearly resolved at the magnification of about 500X (Figure 1(d)), and therefore, for this microstructure, each microstructural frame of the montage should be at a magnification of 500X. In the next step, each microstructural field of the montage is digitally compressed to an equivalent magnification level at which the spatial patterns of the microstructural features of the coarsest length scale of interest are detected. For the A356 alloy microstructure, the coarsest features of interest are the micropores and their spatial patterns can be detected at a magnification of about 25X to 50X (Figure 1(b)), and therefore, each microstructural field (at 500X) in the montage is digitally compressed by a factor of about 10 to 20. Figure 4(a) shows such a montage of 600 digitally compressed images of the microstructure of A356 alloy, which represents six contiguous microstructural fields at a magnification of 50X. These compressed images was created by digital compression of a seamless montage of 600 contiguous microstructural fields at 500X (a part of this 500X montage is shown in Figure 3(b)). The montage shown in Figure 4(a) reveals that the micropores are spatially clustered.

C. *Connected Cascade of FE Schemes at Different Length Scales*

The compressed digital image montage from the digital image analyzer can be imported in a workstation (or PC) to perform the FE element analysis. For this purpose, one needs centroid coordinates of all the micropores (for present microstructure) in the compressed montage, and a set of closely spaced (X, Y) coordinates on the boundary of each micropore, both of which can be obtained in an automatic manner by using commercial image analysis systems. Only the most coarse microstructural features (*i.e.*, micropores in the present case) are resolved in the compressed image montage, and therefore, at this length scale resolution, these coarse features are the only heterogeneities in the structure; the remaining microstructure is modeled as a homogenous *effective* medium. In the compressed image of A356 alloy, the only heterogeneities are the micropores. Strictly speaking,

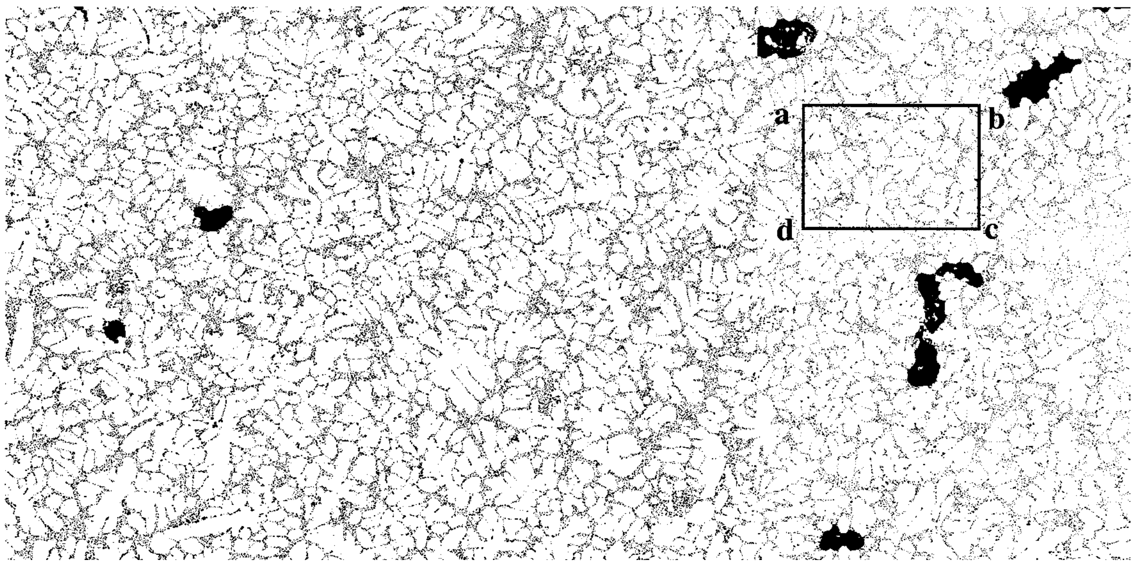

(*a*)

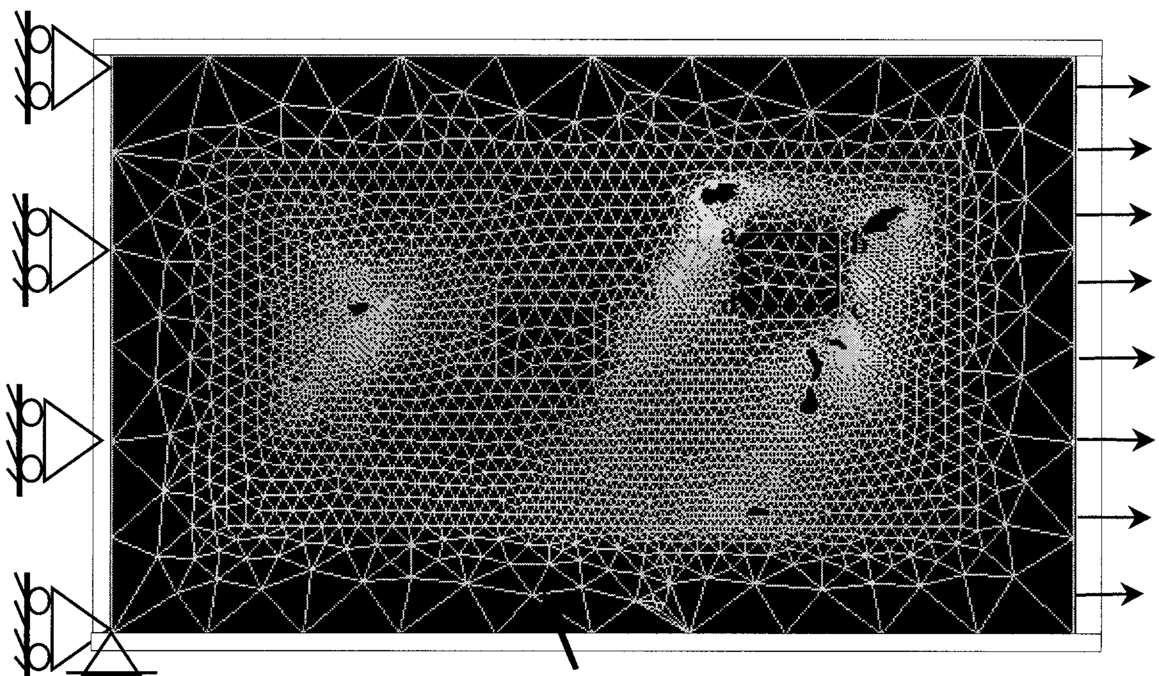

(*b*)

Fig. 4—(*a*) Digitally compressed montage from a montage of 600 contiguous images at 500X. This montage is equivalent to six microstructural fields at 50X. Bordered frame (**abcd**) is for the second-level FE-based simulation. (*b*) FE-mesh and boundary conditions at the length scale level of micropores.

at this length scale, the remaining structure should be modeled as a homogenous effective medium having the properties of the micropore-free A356 alloy. However, the volume fraction of micropores in the present alloy is quite small ($<$0.01). Therefore, as a first approximation, in this simulation, the remaining microstructure is modeled as a homogenous medium having effective properties of the A356 alloy itself (stress-strain curve (b) in Figure 5). The whole compressed image montage is then embedded in a homogeneous effective medium whose stress-strain curve is also assumed to be the same as the overall experimentally measured stress-strain curve for this alloy. Such embedding is essential to decrease the edge effects due to finite boundaries. Figure 4(b) shows the FE mesh overlaid on the compressed microstructural montage, which is embedded in such a homogenous effective medium. Observe that in Figure 4(b), in order to accurately compute the local stresses and strains around the micropores, finer mesh is used in regions around micropores, and a coarser mesh is used in regions that do not contain micropores. In the present work, ABAQUS software is used for the FE analysis on the setup in Figure 4(b). In this simulation, uniaxial displacement of 50 μm is applied in the *X*-direction along the right edge of the frame; this amounts to an applied strain of about 1 pct. Figure 4(b)

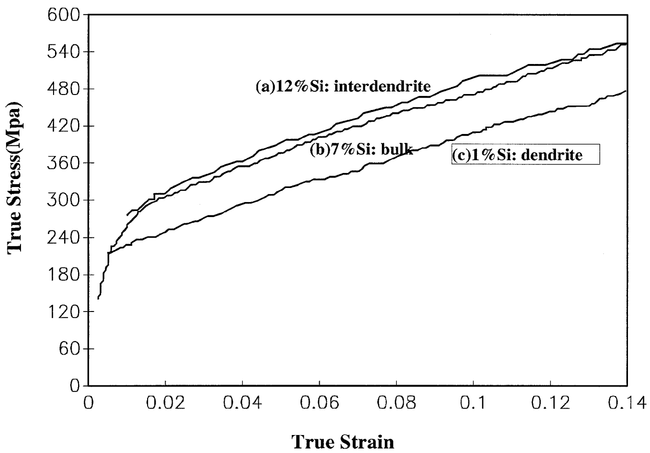

Fig. 5—Stress-strain relations of different aluminum-cast alloys. (*a*) 12 pct Si corresponds to the composition of eutectic alloy (interdendrite region). (*b*) 7 pct Si corresponds to the composition of dendrite cells. (*c*) 1 pct Si is the composition of the A356.

also shows the appropriate rollers and hinge used for the simulation. The appropriate boundary conditions are imposed on the edges of the frame, such that the principle stresses are along the *X* and *Y* axes of the frame. The *X* and *Y* displacements at various points in compressed montage were computed by using ABAQUS code for FE analysis performed on the setup shown in Figure 4(b). These displacements can be converted into local stresses and strains by using standard procedures. For the present simulation, the matrix is assumed to be elastic-plastic (see the stress-strain curve (b) given in Figure 5). Figure 6 shows a contour plot of the distribution of effective plastic strain obtained in this manner. Observe that the local plastic stain is significantly higher in the regions where micropores are clustered. Using similar procedures, one can also obtain contour plots of distribution of maximum principal stress, or any other attributes of local stresses and strains.

Now focus on the bordered region **abcd** in Figures 4(a) and (b). The *X* and *Y* displacements on the boundaries of this frame are precisely known, from the FE analysis on the compressed montage. The pixel coordinates of the end points of this frame are also known, and therefore, one can go back to the *original high magnification seamless montage*, locate the corresponding pixel coordinates, and identify the exact microstructural region that represents the bordered region **abcd** in the compressed montage of Figures 4(a) and (b). This montage segment is then copied in a separate image file. This segment of the high magnification montage may consist of more than one high magnification microstructural field. Now one can digitally recompress (if necessary) this high magnification segment to reveal the spatial pattern of the next length scale microstructural features. In the case of A356 alloy, these features are dendrite cells, and Figure 7 shows the high magnification view of the bordered region **abcd** in Figures 4(a) and (b). As mentioned earlier, the displacements on the boundaries of the microstructural frame in Figure 7 (which is bordered region **abcd** in Figures 4(a) and 4(b)) are known from our first FE simulation on the compressed montage. These displacements now serve as the *boundary conditions* for the second link in the cascade of the FE schemes. These boundary conditions implicitly contain the effect of coarse features (micropores in A356 alloy) on the local stress and strain distributions in the next length scale level features (dendrite cells in A356 alloy). Figure 8 shows the displacements on the boundaries of the frame **abcd** (Figure 7) obtained in this manner, and new FE mesh for the next level FE-based simulation in the cascade. In the A356 alloy, at this level of resolution, the dendrite cells are resolved but the individual silicon particles in the interdendritic regions are not clearly resolved. The interdendritic regions are silicon-rich regions of eutectic composition. Therefore, their constitutive behavior is modeled by using the experimental stress-strain curve of a bulk eutectic alloy* containing 12 pct Si, as given in Figure 5. On the other hand, Al-rich dendrite cells have approximately 1 pct Si, and their constitutive behavior is modeled by using the

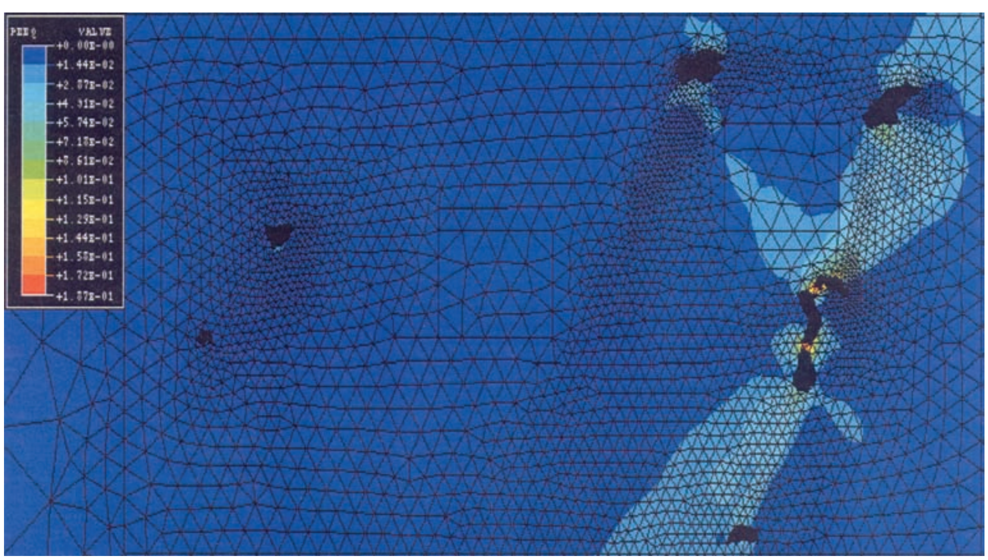

Fig. 6—Distribution of the equivalent plastic strain obtained from simulation in Fig. 4 at the micropore level. Values of equivalent plastic strains greater than zero signify the yielding of material.

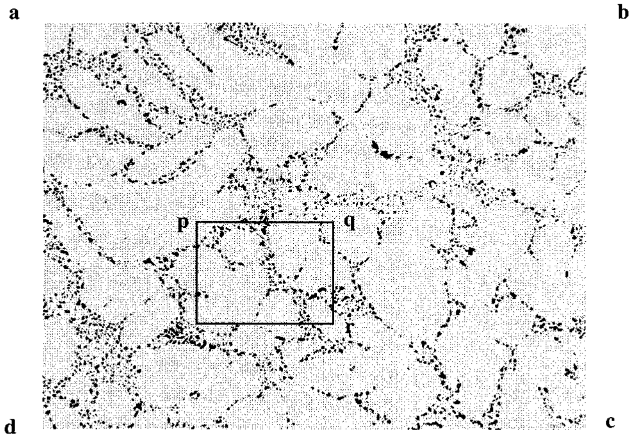

Fig. 7—Real image of the geometric model for the length scale of dendrite cells.

experimental tensile stress-strain curve of a bulk alloy* having 1 pct Si shown in Figure 5. Obviously, both interdendritic regions and Al-rich dendrite cells are modeled as elastic-plastic materials.

*Note that these bulk alloys (both 1 wt pct Si and 12 wt pct Si) were prepared such that the composition of other elements such as Mg, Fe, Cu *etc.* was exactly the same as that in A356 alloy under investigation.

Now, focus on bordered region **pqrs** in Figure 7 and the corresponding digital image in Figure 9. The displacements at the boundaries of this region are precisely known from our second level simulation (Figure 8). The pixel coordinates of the corners of the bordered region are also known from the digital image in Figure 7. One can again go back to the original seamless high magnification montage and identify the corresponding pixel coordinates and the high magnification segment of the seamless montage that constitute the bordered region **pqrs** in Figure 7. Figure 9 is the high magnification view of this bordered region **pqrs** in Figure 7. This high magnification image is one field of view at 500X (the magnification at which the original images were grabbed), and it clearly reveals the Si particles which are the finest length scale of interest. As mentioned earlier, the displacements at the boundaries of this frame are precisely known from the second level simulation. These displacements are used as boundary conditions (Figure 10) for the next level simulation, *i.e.*, the length scale of silicon particles for the A356 cast alloy. Recall that the FE simulation is performed on the digital image of Figure 9. These boundary conditions implicitly account for the effect of the dendrite cells, *and* micropores on the local displacements, strains, and stresses around individual silicon particles in this frame. Figure 11 depicts the distribution of effective plastic strains around the individual silicon particles. The extremely high equivalent plastic strains among the silicon particles may cause the void nucleation and coalescence, which is critical to the deformation and fracture of the alloy. In this third-level simulation, the effects of the micropores (that are present at length scales of 200 to 500 μm), dendrite cells, and the silicon particles, on the stresses and strains around silicon particles that at the length scale of 3 to 5 μm are incorporated. In this manner, the microstructural length scales that differ by two orders of magnitude have been successfully linked. In the third-level FE analysis, the silicon particles are modeled as completely elastic, and the matrix is modeled as an elastic-plastic material. The constitutive behavior of the matrix is assumed to be that of 1 wt pct silicon alloy.* The stress-strain curve is given in Figure 5. Further, it is assumed that there is a perfect bond at the interfaces of the silicon particles, and therefore, this simulation does not treat any debonding at the silicon particle interfaces. However, in principle, it is possible to incorporate this damage mechanism if the properties of the silicon particle interface are known.

All the present FE simulations are on the actual digital images of the microstructure, and therefore, they automatically account for the actual nonuniform spatial arrangement of microstructural features present at different length scales. It is very important to recognize the FE mesh size around the silicon particles in the third-level simulation shown in Figure 10. It is about two orders of magnitude finer than that in the first-level simulation shown in Figure 4. If the cascading of FE schemes is not used, then it would be necessary to use such a fine mesh in the original high magnification montage. It would take a tremendous amount of effort to create such a fine mesh over such a large area of the original montage, and such simulation would be computationally extremely *inefficient*. In the present example of A356 alloy, cascading of the FE reduces the computations by more than two orders of magnitude. To characterize the effect of spatially clustered micropores on the local stress and strain distributions around silicon particles, the second- and third-level FE simulations can be repeated on the different regions in the original compressed digital image.

IV. RESULTS AND DISCUSSION

In this contribution, a digital image processing technique is presented to perform the FE analysis directly on the digital images of microstructure at different length scales, *and* to link the interactions of the microstructural features whose length scales may differ by two or three orders of magnitude. The procedure simply involves merger of two tools, namely, digital image processing and FE analysis. The practical feasibility of the procedure is demonstrated *via* an application to multi–length scale microstructure of a common commercial Al-Si-Mg base cast alloy (A356), where the length scale of micropores and silicon particles differs by about two orders of magnitude. It is possible to extend this technique to link the length scales on the order of the dimensions of the actual tensile test specimen (~ few cm) to the length scales on the order of 5×10^{-5} cm (*i.e.*, 0.5 μm), which is close to resolution limit of the optical microscopy. If the image analyzer is linked to scanning electron microscopy, then it should be possible to go to even lower length scales. However, at the present level of technology, it is practically *not* feasible to extend the methodology down to the length scales of dislocations, and therefore, homogenization (so called, "smearing" of structure) at very low length scales is still required. The method is primarily useful to model the effect of the microstructural features at higher length scales on the damage evolution and local fracture mechanisms that operate at much lower length scales. The main advantage of the method is that the spatial arrangements of microstructural features, spatial patterns, and correlations at different length scales are captured in the FE analysis, and therefore, it should

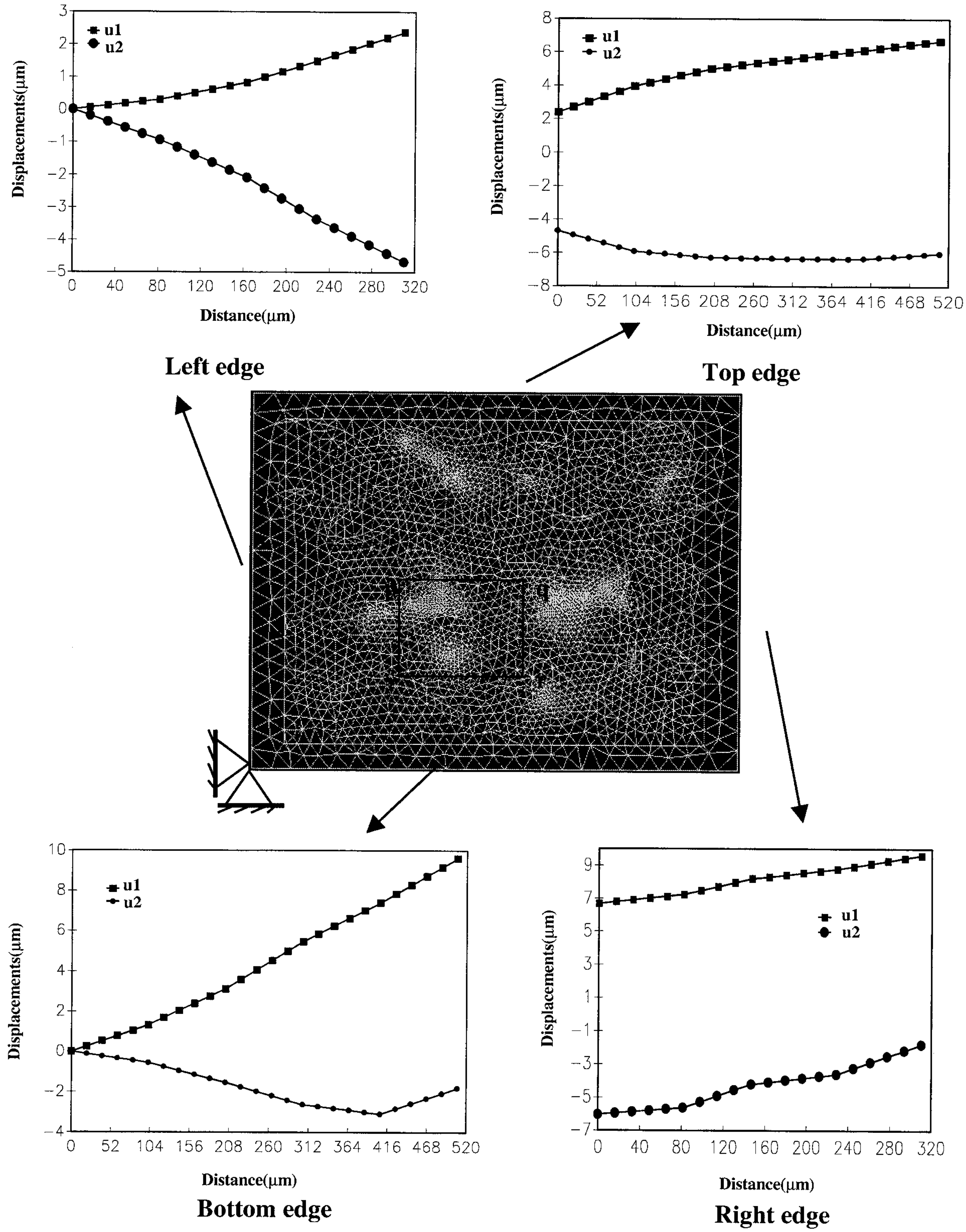

Fig. 8—FE mesh and boundary conditions at the length scale of dendrite cells. (Fig. 7).

enable development of realistic models for damage evolution and fracture mechanisms at lower length scales that can be applied to complex real material microstructures.

An important advantage of cascading of the FE schemes is the resulting efficiency in the creation of meshes and the computational efficiency. To perform FE analysis and micromechanical calculations on the irregular (*i.e.*, real) microstructures, the FE meshes have been created manually, which is a quite time-consuming process. Further, to capture the local displacement distributions around fine features (like

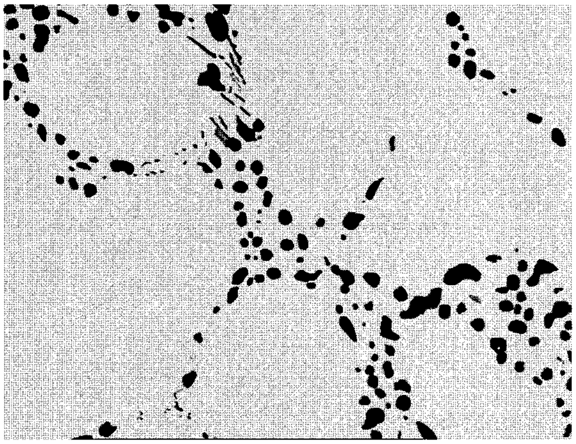

Fig. 9—Digital image showing silicon particles in the interdendritic region.

Si particles in the A356 alloy) having length scales on the order of a micron or so, the mesh sizes have to be finer than a micron or so. It would take a lot of effort to create such fine meshes over a large area ($\sim$ few mm^2). This problem is significantly lessened by the cascading of the FE schemes. For example, the mesh in Figure 4(b) is coarse, and the successive links in the cascade have finer and finer meshes. Therefore, it is not necessary to overlay the whole area of the initial microstructural montage with very fine mesh.

For successful application of the technique, *a priori* information on the homogenous medium properties at a number of different levels is required. In the case of A356 alloy, the experimentally measured *local* mechanical properties of the interdendritic eutectic region, aluminum-rich dendrites, and Si particles are desirable for a detailed FE analysis and micromechanics/damage mechanics based modeling of the damage evolution and local fracture processes. Such mechanical properties data are required for conventional micromechanical calculations as well. In the present simulations, as an approximation, properties of a *bulk* cast alloy containing 12 wt pct Si have been used to model the interdendrite regions, a *bulk* cast alloy containing 1 pct Si has been used to model the constitutive behavior of the Al-rich dendrites, and Si has been assumed to be a perfectly elastic material. The main objective of this contribution is to present the basic Microstructural Scale Linking by Image Processing (M-SLIP) technique, and not detailed micromechanical/damage mechanics computations. The derailed micromechanics based modeling of silicon particle fracture and damage evolution will be presented in a subsequent article.

In Figures 4(a) and (b), the bordered region (**abcd**) for the second-level FE analysis were selected near the clustered micropores. Similar calculations can also be done on the frames selected at different locations in the compressed montage to characterize the effect of the spatial arrangement of micropores on the local stresses and strains around the silicon particles. The local spatial arrangement of micropores has significant influences on the displacement fields. Figure 12 is the contour plot of the displacement fields at the length scale of micropores. The displacement field varies with location due to the presence of micropores. Figure 13(a) shows two microstructural frames at different locations in the compressed montage, and Table I shows the corresponding average displacements at the boundaries of these two microstructural frames. Frame A (which is at same location as **abcd** in Figures 4(a) and (b)) is in the vicinity of the clustered micropores, and the frame B is in the region away from micropores (Figure 13(a)). Table I illustrates that the displacements at the boundaries of the two frames are quite different. These differences in the displacements (which are the boundary conditions for the second-level FE analysis) lead to differences in the local stress and strain distributions in the two microstructural fields. Local stresses and strains around silicon particles depend on the local spatial distribution of the silicon particles (which may vary from one field to another) and relative vicinity of the micropores at higher length scale. To deconvolute these two contributions, and to bring out the effect of the spatial clustering of micropores on the stresses and strains around Si particles, the *same* high magnification microstructural field was embedded at the two different locations in frame A and frame B in Figure 13(a), and simulations were performed. Figures 13(b) and (c) show the equivalent plastic strain distributions around the Si particles at the two locations obtained from these simulations. It can be seen that significant deformation has occurred in the microstructural field which is in frame A Figure 13(c). Most of the regions in this field have the equivalent plastic strains significantly higher than zero. However, for the same microstructural field embedded in frame B, the equivalent plastic strain (Figure 13(b)) is significantly lower than its counterpart in frame A (Figure 13(c)). These differences in the strains (and stresses) are expected to influence the damage evolution of silicon particles in these locations.

The combination of the image processing techniques and the FE analysis presented in this article basically pertains to a two-dimensional section through a three-dimensional material microstructure and associated two-dimensional FE analysis, although the material microstructures are three-dimensional. It is important to point out that most of the micromechanics/damage mechanics based modeling studies based on FE analysis that are reported in the literature have been performed on two-dimensional microstructure. It is not known whether such two-dimensional simulations capture all the salient features of the mechanical response of three-dimensional material microstructures. However, there has been some progress during the last few years in the development of three-dimensional FE analysis methods that can be used for micromechanical modeling studies.[6] In principle, it is possible to extend the present methodology to three-dimensional microstructures. For this purpose, a serial sectioning of the microstructure is necessary to generate a large volume "montage" of three-dimensional microstructure. Such a three-dimensional microstructural montage can be then utilized as an input for the three-dimensional FE analysis that can be used to model micromechanics/damage mechanics based response of the complex multi–length scale material microstructures.

In general, the M-SLIP technique enables the incorporation of the effects of the higher length scale microstructural features on the damage of lower length scales in the FE-based simulations of the mechanical response of multi–length scale microstructures. Furthermore, more realistic parametric studies can be performed. For example, in the A356 cast alloy, the effects of changing the sizes of micropores present at higher length scales on the damage of silicon particles at

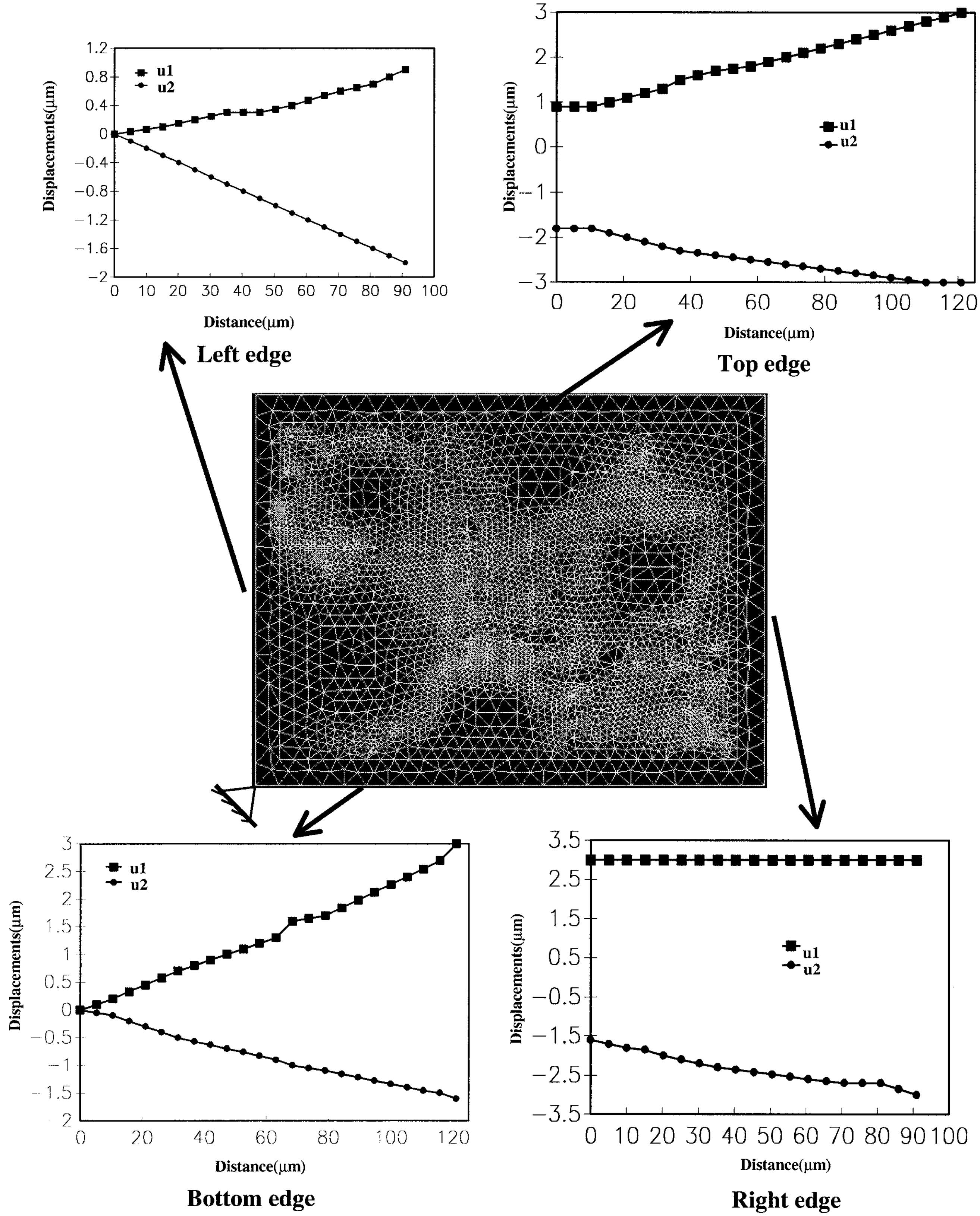

Fig. 10—FE mesh and boundary conditions at the length scale of silicon particles (Fig. 9).

lower length scales can be studied without changing the spatial arrangement of the micropores. Therefore, the parametric study is more related to the actual situation. As a result, the M-SLIP technique provides an alternative way to the homogenization method to account for the existence of different length scales in material microstructure. This

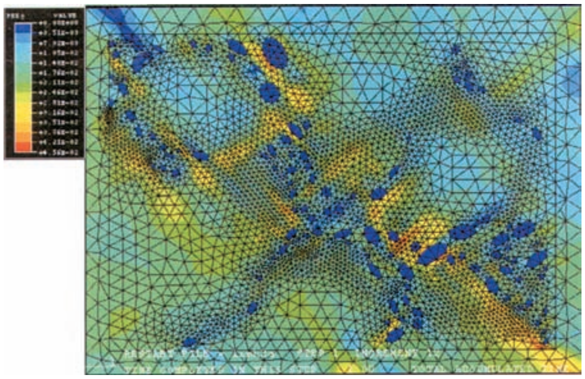

Fig. 11—Contour plot of equivalent plastic strains obtained from FE simulation in Fig. 10 at length scale of silicon particles.

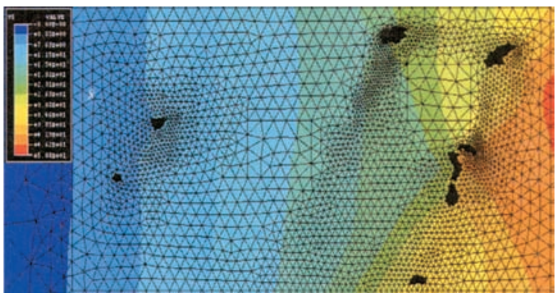

Fig. 12—Contour plot of the displacement field at the length scale of micropores. It shows the variation of the displacements due to the presence of the micropores.

Table I. Average Displacements along the Edges of the Two Frames (Frame A and Frame B) in Figure 13(a)

Frame	Left (μm)	Right (μm)	Difference (u_1)(μm)	Top (μm)	Bottom (μm)	Difference (u_2)(μm)
A	22.73	29.83	7.10	−11.86	−7.53	−4.33
B	13.04	16.41	3.37	−6.90	−5.24	−1.66

technique is essential in FE-based modeling of the mechanical response of nonuniform multi–length scale microstructures.

V. SUMMARY AND CONCLUSIONS

The M-SLIP technique involves combination of image analysis and cascading of FE schemes. It provides a powerful tool for quantification of local stresses and strains around heterogeneities in the complex multi–length scale microstructures. The technique is useful to account for the effect of heterogeneities at higher length scales on the damage and fracture processes at lower length scales. The resulting stresses and strains can be used for the micromechanics/damage mechanics based modeling studies of damage evolution/fracture. As the FE analysis is performed on the digital image of the microstructure, the technique automatically incorporates the effect of size, shape, orientations, and spatial arrangements of the microstructural features at different length scales in the FE analysis. Therefore, the technique is useful for modeling the mechanical response of complex multilength microstructures of the engineering alloys.

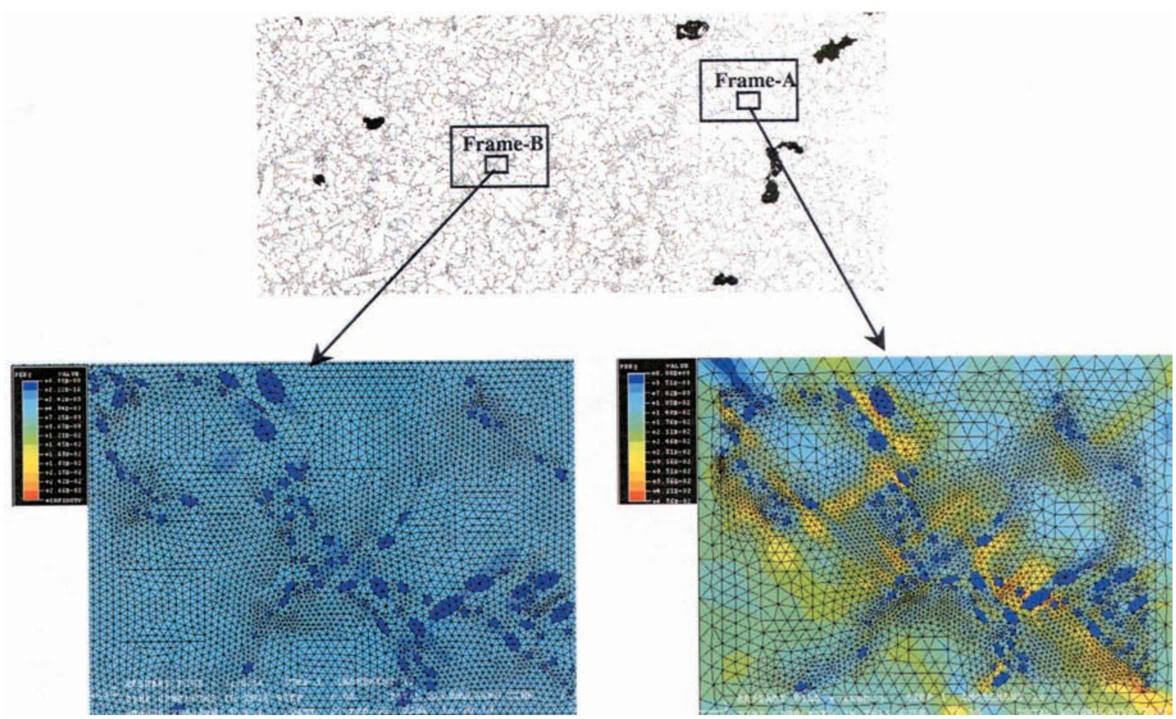

Fig. 13—Distributions of equivalent plastic strains around the silicon particles for same microstructural field, but at different locations: (*a*) compressed digital montage showing frame A and frame B; (*b*) distribution of equivalent plastic strains when the field is in frame B; and (*c*) distribution of equivalent plastic strains when the field is in frame A.

ACKNOWLEDGMENTS

This research work is supported by U.S. National Science Foundation Research Grant No. DMR-9816618, for which Dr. B. MacDonald is the Program Monitor. The financial support is gratefully acknowledged. The authors also thank Professor D.L. McDowell and Dr. Mark Horstemeyer for numerous useful discussions.

REFERENCES

1. Jien-Wei Yeh and Wen-Pin Liu: *Metall. Mater. Trans. A*, 1996, vol. 27A, pp. 3558-68.
2. N. Roy, A.M. Samuel, and F.H. Samuel: *Metall. Mater. Trans. A*, 1996, vol. 27A, pp. 415-29.
3. A.M. Gokhale, M.D. Dighe, and M. Horstmeyer: *Metall. Mater. Trans. A*, 1998, vol. 29A, pp. 905-08.
4. C.H. Caceres and J.R. Griffiths: *Acta Mater.* 1996, vol. 44, pp. 25-33.
5. M.D. Dighe and A.M. Gokhale: *Scripta Mater.*, 1997, vol. 37, pp. 1435-40.
6. M. Oritz: *Comp. Mech.*,1996, vol. 15, pp. 321-38.
7. C. Ruggieri, T.L. Panontin, and R.H. Dodds, Jr.: *Int. J. Fract.*, 1996, vol. 82, pp. 67-95.
8. J. Fish and A. Wagiman: *Comp. Mech.*, 1993, vol. 12, pp. 1-17.
9. Min Zhou, A. Needleman, and R.J. Clifton: *J. Mech. Phy. Solids*, 1994, vol. 42, pp. 423-8.
10. L. Llorca, A. Needleman, and S. Suresh: *Acta Metall. Mater.*, 1991, vol. 39, pp. 2317-35.
11. Th. Steinkopff and M. Sautter: *Comp. Mater. Sci.*, 1995, vol. 4, pp. 15-22.
12. M. Dong and S. Schmaunder: *Acta Mater.*, 1996, vol. 44, pp. 2465-78.
13. P.M. Lesne, N. Allio, and R. Valle: *Acta Mater.*, 1995, vol. 43, pp. 4247-66.
14. M.D. Dighe and A.M. Gokhale: *Scripta Mater.*, 1997, vol. 37, pp. 1435-40.
15. P. Louis and A.M. Gokhale: *Acta Metall. Mater.*, 1996, vol. 44, pp. 1519-28.
16. Pascal Louis and A.M. Gokhale: *Metall. Mater. Trans. A*, 1995, vol. 26A, pp. 1449-56.
17. J.R. Brokenbrough and W.H. Hunt: *Scripta Metall. Mater.*, 1992, vol. 27, pp. 385-90.
18. J. Wulf, T. Steinkopff, and H.F. Fischmeister: *Acta Mater.*, 1996, vol. 44, pp. 1765-79.
19. J.R. Rice and M.D. Tracy: *J. Mech. Phy. Solids*, 1969, vol. 17, pp. 201-10.
20. A. Al-Ostaz and I. Jasiuk: *Acta Mater.*, 1997, vol. 45, pp. 4131-43.